Nonaffine Deformation of Semiflexible Polymer and Fiber Networks

Sihan Chen, Tomer Markovich, and Fred C. MacKintosh

Non-affine deformation of semiflexible polymer and fiber networks

Sihan Chen[1,2], Tomer Markovich[2,3,4], Fred C. MacKintosh[1,2,5,6]

[1]*Department of Physics and Astronomy, Rice University, Houston, TX 77005*
[2]*Center for Theoretical Biological Physics, Rice University, Houston, TX 77005*
[3]*School of Mechanical Engineering, Tel Aviv University, Tel Aviv 69978, Israel*
[4]*Center for Physics and Chemistry of Living Systems, Tel Aviv University, Tel Aviv 69978, Israel*
[5]*Department of Chemical and Biomolecular Engineering, Rice University, Houston, TX 77005*
[6]*Department of Chemistry, Rice University, Houston, TX 77005*

Networks of semiflexible or stiff polymers such as most biopolymers are known to deform inhomogeneously when sheared. The effects of such non-affine deformation have been shown to be much stronger than for flexible polymers. To date, our understanding of non-affinity in such systems is limited to simulations or specific 2D models of athermal fibers. Here, we present an effective medium theory (EMT) for non-affine deformation of semiflexible polymer and fiber networks, which is general to both 2D and 3D and in both thermal and athermal limits. The predictions of this model are in good agreement with both prior computational and experimental results for linear elasticity. Moreover, the framework we introduce can be extended to address nonlinear elasticity and network dynamics.

Networks of stiff or semiflexible polymers are vital for the function of most living systems. Such networks control much of the elastic properties of biomaterials ranging from the cell cytoskeleton to extracellular matrices at the tissue scale [1–4]. Over the past few decades there has been significant progress in our understanding of the fundamental physical properties of semiflexible networks [5–17]. Previous studies of 2D and 3D semiflexible networks have, among other things, revealed a transition from bend-dominated, non-affine regime to a stretch-dominated, affine regime [18–28] that is governed by the average polymer length (or molecular weight), in stark contrast with flexible polymer systems.

The classical theory of *rubber elasticity* [29–31] is very successful in describing the elastic properties of flexible polymers networks. Early approaches assumed deformations to be affine, with uniform strain on all scales. The phantom-network model relaxed this assumption and showed that local network structure indeed affects elastic properties, but in a way that does not change the basic scaling with macroscopic quantities such as average polymer length, system volume, temperature, etc. [32–34]. By contrast, the strong bending rigidity of semiflexible polymers invalidates the phantom model and leads to much stronger non-affine effects [18, 19, 35], including a surprising dependence on dimensionality [22]. Most of the prior work accounting for non-affinity in semiflexible networks has been limited to numerical simulation [20, 36–39], while a theory analogous to the phantom network has been lacking, especially in 3D. Various models based on effective medium theories (EMT) introduced for rigidity percolation [40–42] have been proposed for lattice-based or topologically similar networks [21, 24, 43–48], along with floppy mode models for off-lattice networks [49, 50]. But, both of these approaches have been limited to 2D networks and have neglected important thermal fluctuations.

Here, we develop an analytical model for the elasticity of both thermal semiflexible polymer and athermal fiber networks that accounts for the non-affine deformations. Our model applies to both lattice-based and random off-lattice networks that are isotropic and homogeneous on large scales. As we show, this model can be applied to both thermal and athermal networks. Our prediction of the bend-to-stretch transition quantitatively agrees with previous athermal simulations of 3D networks, while explaining the different scaling dependences on filament length in 2D lattice and off-lattice (e.g., Mikado) networks. Moreover, for thermal networks where simulations are lacking, our model predicts a bend-to-stretch transition that agrees with previous experiments [26, 51]. Although we focus here on the linear elastic limit, this model can also be extended to address the role of non-affine fluctuations in the dynamics [52–55], stress-stiffening [11, 12] and recently identified strain-controlled criticality [56–59].

We begin by considering an athermal crosslinked semiflexible polymer network in 3D. The discussion on 2D and thermal networks is postponed to later. The network is formed by N filaments each with polymer length L and point-like hinged crosslinks with average crosslinking distance ℓ_c. Its Hamiltonian is:

$$H_O = \sum_{\alpha=1}^{N} \left[H_b\left[\boldsymbol{u}^\alpha(s)\right] + H_s\left[\boldsymbol{u}^\alpha(s)\right] \right], \qquad (1)$$

where $\boldsymbol{u}^\alpha(s) = \boldsymbol{u}_\parallel^\alpha(s) + \boldsymbol{u}_\perp^\alpha(s)$ is the microscopic displacement of the α-th polymer at position s along its contour ($-L/2 < s < L/2$), with $\boldsymbol{u}_\parallel^\alpha(s)$ and $\boldsymbol{u}_\perp^\alpha(s)$ being its longitudinal and transverse components, respectively. $H_b\left[\boldsymbol{u}(s)\right] = \kappa \int \mathrm{d}s |\partial^2 \boldsymbol{u}_\perp/\partial s^2|^2/2$ and $H_s\left[\boldsymbol{u}(s)\right] = \mu \int \mathrm{d}s |\partial \boldsymbol{u}_\parallel/\partial s|^2/2$ are the bending and stretching energy, respectively. If a crosslink exists between the α-th and the β-th polymer, it leads to an additional constraint, $\boldsymbol{u}^\alpha(s_{\alpha\beta}) = \boldsymbol{u}^\beta(s_{\beta\alpha})$, with $s_{\alpha\beta}$ ($s_{\beta\alpha}$) being the position of
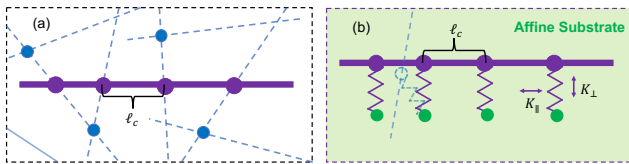
Figure 1. (a) 2D sketch of a crosslinked semiflexible polymer network in either 2D or 3D, with average crosslinking distance ℓ_c. Each polymer has a contour length L. (b) Sketch of the EMT, in which crosslinks are replaced by springs that connects the polymers with a substrate which deforms affinely (two polymers connected by one crosslink are connected to the substrate via two different springs, see, e.g., the dashed polymer). Spring constants for the parallel and transverse directions of the connected polymer are $K_\parallel$ and $K_\perp$, respectively.

the crosslink on the α-th (β-th) polymer.

We are interested in how this network deforms under an external shear stress σ_O. For athermal networks the deformation is found from the minimum-energy state, in which the microscopic deformations of each polymer are denoted by $\widetilde{\boldsymbol{u}}^\alpha(s)$ and the shear strain of the entire network is γ_O. The linear shear modulus is defined as $G_O = \partial\sigma_O/\partial\gamma_O|_{\gamma_O=0}$. For simplicity we assume a stress σ_O in the $x-z$ plane. This causes (in the linear regime) a simple shear of the $x-z$ plane in the x direction, such that γ_O corresponds to a single nonzero term $\Lambda_{xz} = \gamma_O$ in the deformation tensor $\underline{\boldsymbol{\Lambda}}$.

Although the network Hamiltonian has a quadratic form (Eq. (1)), a direct analytical solution of the minimum-energy state is challenging for two reasons: the first is the existence of the crosslinking constraints, which introduces correlations between different polymers. Therefore, their deformations $\boldsymbol{u}^\alpha(s)$ can not be considered as independent variables; the other is the unclear relation between the microscopic deformations ($\boldsymbol{u}^\alpha$) and the macroscopic deformation (γ_O) for non-affine deformations. Below we detail how we overcome these challenges.

To remove the crosslink constraints, we have developed an EMT, in which all the polymers in the original network are preserved while all crosslinks are removed (Fig. 1(b)). To mimic the restraining effect of the crosslinks, each crosslink is replaced by a spring that connects the polymer at the position of the crosslink with a substrate. The substrate can only deform affinely, and its deformation does not cost any energy. Each spring has two spring constants, $K_\parallel$ and $K_\perp$, for the parallel and transverse direction of its connected polymer, respectively. The resulting EMT has an additional elastic energy H_K and the effective Hamiltonian is

$$H_{\mathrm{EM}} = \sum_{\alpha=1}^{N} \Big(H_b\left[\boldsymbol{v}^\alpha(s)\right] + H_s\left[\boldsymbol{v}^\alpha(s)\right] + H_K\left[\boldsymbol{v}_{\mathrm{NA}}^\alpha(s)\right] \Big), \tag{2}$$

where the microscopic deformation in the EMT is denoted by $\boldsymbol{v}^\alpha(s) = \boldsymbol{v}_A^\alpha(s) + \boldsymbol{v}_{\mathrm{NA}}^\alpha(s)$, with $\boldsymbol{v}_A^\alpha(s)$ being the affine displacement and $\boldsymbol{v}_{\mathrm{NA}}^\alpha(s)$ being the non-affine displacement. Note that only non-affine displacements affect H_K, since forces are not induced between affinely deforming polymers that simply stretch/compress uniformly. The microscopic affine displacements are given by $\boldsymbol{v}_A^\alpha(s) = s\underline{\boldsymbol{\Lambda}} \cdot \hat{\boldsymbol{n}}^\alpha$, with $\hat{\boldsymbol{n}}^\alpha$ defining the polymer orientation. The additional energy H_K is the summation of the elastic energy of all springs connected to each polymer:

$$H_K\left[\boldsymbol{v}_{\mathrm{NA}}^\alpha(s)\right] = \frac{K_\parallel}{2} \sum_i |\boldsymbol{v}_{\mathrm{NA}\parallel}^\alpha(s_i)|^2$$
$$+ \frac{K_\perp}{2} \sum_i |\boldsymbol{v}_{\mathrm{NA}\perp}^\alpha(s_i)|^2, \tag{3}$$

where s_i is the position of the i-th spring, and $v_{\mathrm{NA}\perp}^\alpha$ and $v_{\mathrm{NA}\parallel}^\alpha$ are the transverse and longitudinal components of v_{NA}^α, respectively. Importantly, terms with the same index α in Eq. (2) describe a single-polymer Hamiltonian in which the network structure is accounted for through a harmonic energy. Such approach is conceptually similar to the effective spring constant introduced in Refs. [60, 61] for entangled polymer solutions, as well as tube models for flexible polymer networks [62].

Under an imposed shear stress σ_{EM}, we define the microscopic deformations in the minimum-energy state of the EMT as $\widetilde{\boldsymbol{v}}^\alpha(s)$, with a shear strain γ_{EM} and an elastic modulus $G_{\mathrm{EM}} = \partial\sigma_{\mathrm{EM}}/\partial\gamma_{\mathrm{EM}}|_{\gamma_{\mathrm{EM}}=0}$. Our goal is to find an EMT that reproduces the elasticity of the original network on average, i.e. $G_{\mathrm{EM}} = G_O$, the inverse of which can be rewritten using the chain rule:

$$\sum_{\alpha i} \frac{\partial\widetilde{\boldsymbol{u}}_i^\alpha}{\partial\sigma_O} \cdot \frac{\partial\gamma_O}{\partial\widetilde{\boldsymbol{u}}_i^\alpha} = \sum_{\alpha i} \frac{\partial\widetilde{\boldsymbol{v}}_i^\alpha}{\partial\sigma_{\mathrm{EM}}} \cdot \frac{\partial\gamma_{\mathrm{EM}}}{\partial\widetilde{\boldsymbol{v}}_i^\alpha}, \tag{4}$$

where $\widetilde{\boldsymbol{u}}_i^\alpha = \widetilde{\boldsymbol{u}}^\alpha(s_i)$ and $\widetilde{\boldsymbol{v}}_i^\alpha = \widetilde{\boldsymbol{v}}^\alpha(s_i)$ are the displacements on the crosslink positions (symbols without tilde are arbitrary polymer displacements, while symbols with tilde denote polymer displacements in the minimum-energy state). To ensure that Eq. (4) is satisfied, we look for an EMT that satisfies simultaneously

$$\left\langle \frac{\partial\widetilde{\boldsymbol{u}}_i^\alpha}{\partial\sigma_O} \right\rangle = \frac{\partial\widetilde{\boldsymbol{v}}_i^\alpha}{\partial\sigma_{\mathrm{EM}}}, \tag{5a}$$

$$\frac{\partial\gamma_O}{\partial\widetilde{\boldsymbol{u}}_i^\alpha} = \frac{\partial\gamma_{\mathrm{EM}}}{\partial\widetilde{\boldsymbol{v}}_i^\alpha}. \tag{5b}$$

In Eq. (5a) we average the effects of random crosslinking angles in the original network. These requirements may not be the only appropriate ones and may appear to be stronger than necessary. However, as we will show later, this choice does lead to good agreement with the expected macroscopic elasticity. Equation (5a) is essentially a coherent potential approximation (CPA) as in
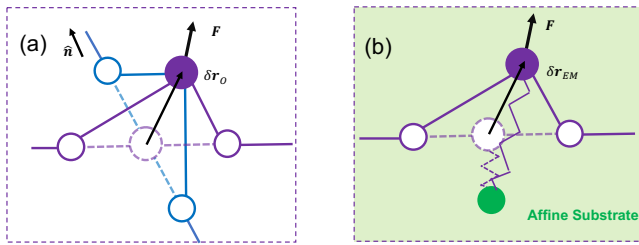
Figure 2. Sketch of the test force approach. A particular node on the purple polymer is deformed by a test force $\boldsymbol{F}$. The resulting displacement is $\delta\boldsymbol{r}_O$ in the original network (a), and $\delta\boldsymbol{r}_{\mathrm{EM}}$ in the EMT (b). For 3D networks the adjacent nodes are assumed to be fixed, while for 2D networks the displacement of adjacent nodes need to be considered, see Fig. 4(a).

the classic EMT of 2D lattice-based networks [42, 63]. Importantly, Eq. (5b) is different from what is usually done in an EMT, in that it allows our EMT to deform non-affinely.

We start with the first requirement. Equation (5a) describes the local displacement caused by the stress, which can thus be considered as a local compliance. As the stress can be decomposed to local forces on each node in the network, we exert a test force $\boldsymbol{F}$ on a particular node on the same polymer in both the original network and the EMT, and measure the resulting displacements, $\delta\boldsymbol{r}_O$ and $\delta\boldsymbol{r}_{\mathrm{EM}}$ (see Fig. 2). By letting $\langle\delta\boldsymbol{r}_O\rangle_{\hat{n}} = \delta\boldsymbol{r}_{\mathrm{EM}}$, where $\hat{n}$ is the orientation of the other polymer crosslinked to the node in the original network, we obtain the values of the two spring constants, which for 3D networks read (see Sec. I of [63]):

$$K_\perp = K_\parallel = \frac{18\kappa}{\ell_c^3}. \qquad (6)$$

The equality of $K_\perp$ and $K_\parallel$ is consistent with an isotropic effective medium. Importantly, however, the node compliance is still highly anisotropic due to H_s. Note that in deriving Eq. (6) we assumed for simplicity that all polymers are straight in the undeformed state of the original network. This assumption may not hold in real networks but is consistent with previous lattice-based simulations [15, 22]. We discuss this further in Sec. IC of [63].

To solve Eq. (5b), one needs to find the relation between the macroscopic deformation $\underline{\boldsymbol{\Lambda}}$ and the microscopic deformations $\boldsymbol{u}^\alpha$. This is simple in the affine limit, as noted above. For non-affine deformations the situation is more complex. To address this, instead of determining $\boldsymbol{u}^\alpha$ from $\underline{\boldsymbol{\Lambda}}$, we do it inversely by determining $\underline{\boldsymbol{\Lambda}}$ from $\boldsymbol{u}^\alpha$. Generally, $\underline{\boldsymbol{\Lambda}}$ is a functional of all microscopic deformations, $\underline{\boldsymbol{\Lambda}}\left[\boldsymbol{u}^1(s), \boldsymbol{u}^2(s), ..., \boldsymbol{u}^N(s)\right]$. In the small strain limit, we can always perform a linear expansion,

$$\underline{\boldsymbol{\Lambda}} = \sum_\alpha \int_{-L/2}^{L/2} \mathrm{d}s\, \boldsymbol{u}^\alpha(s) \cdot \underline{\underline{\boldsymbol{T}}}^\alpha(s), \qquad (7)$$
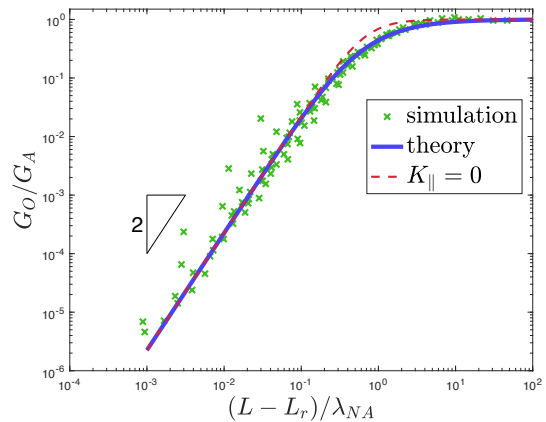

Figure 3. Shear modulus for 3D athermal networks. Simulation results of phantom-fcc-lattice network is reproduced from Ref. [22], with filament length corrected by the minimum length of rigidity percolation, $L_r = 2.85\ell_c$. Theoretical prediction is plotted using Eq. (S41) in Ref. [63], which is similar to Eq. (8) but calculated for networks with exponential length distribution as in the simulation.

where $\underline{\underline{\boldsymbol{T}}}^\alpha(s)$ is a third-order coefficient tensor. We find that $\underline{\underline{\boldsymbol{T}}}^\alpha(s)$ can be uniquely determined from three conditions: (i) the affine deformation should satisfy Eq. (7), as it is a special case of the non-affine deformation; (ii) we assume the network is homogeneous on large scale, so all polymers are identical to each other except for their different orientations, leading to $\underline{\underline{\boldsymbol{T}}}^\alpha(s) = \underline{\underline{\boldsymbol{T}}}(\hat{n}^\alpha, s)$; (iii) we assume the network is isotropic [64]. The full derivation of $\underline{\underline{\boldsymbol{T}}}$ is detailed in Sec. II of [63]. A similar macroscopic-microscopic relation can be defined for the EMT as well with a coefficient tensor $\underline{\underline{\boldsymbol{T}}}_{\mathrm{EM}}^\alpha(s)$, whose value is related to $\underline{\underline{\boldsymbol{T}}}^\alpha(s)$ via Eq. (5b). For 3D networks $\underline{\underline{\boldsymbol{T}}}_{\mathrm{EM}} = \underline{\underline{\boldsymbol{T}}}$, while for 2D networks $\underline{\underline{\boldsymbol{T}}}_{\mathrm{EM}}$ becomes more complicated due to the *floppy mode* deformation [49], see discussion later.

By solving Eqs. (5a) and (5b), we have linked the EMT to the original network. The EMT elasticity G_{EM} can be found by minimizing Eq. (2) under an applied stress, which should be consistent with the elasticity of the original network G_O (see Sec. III A of Ref. [63] for details). For 3D athermal monodispersed networks (all polymers have the same length) we find that

$$\frac{G_O}{G_A} = \left[1 + \frac{4\sqrt{2}\lambda_{\mathrm{NA}}}{L} \cdot \coth\left(\frac{3L}{\sqrt{2}\lambda_{\mathrm{NA}}}\right)\right]^{-1}, \qquad (8)$$

where $G_A = \rho\mu/15$ is the affine linear elastic modulus, ρ is the polymer length density and $\lambda_{\mathrm{NA}} = \ell_c^2/\sqrt{\kappa/\mu}$ is a characteristic non-affine lengthscale. We compare this theoretical prediction with previous simulations on lattice-based 3D networks [22] and find good quantitative agreement in both the scaling for small polymer length L ($G_O \sim L^2$) and in the transition to an affine deformation regime for larger L (Fig. 3). Interestingly, the non-affinity in the EMT is dominated by $K_\perp$. For comparison

we also plot in Fig. 3 the predicted modulus with $K_\parallel = 0$, showing a minor difference in the non-affine/affine transition region. This shows that the longitudinal deformation of the polymers is dominated by their own stretching rigidity, while $K_\parallel$ has a minor effect, mainly in the non-affine/affine transition where almost all longitudinal deformation is achieved from bending surrounding polymers. For simplicity we neglect $K_\parallel$ hereafter.

Having verified our EMT using previous simulations on athermal networks, we consider thermal networks for which simulations are challenging computationally. Such challenge is due to the thermal fluctuations of the network state around its ground state, which are crucial to the elasticity of cytoskeletal networks [11, 12]. The elasticity can be found by calculating the average strain of the Boltzmann distribution at finite temperature T (see Sec. III B of Ref. [63]):

$$G_O = \frac{\rho \mu_{\mathrm{ph}}}{15} \left(1 + 266.7 \ell_c \ell_p / L^2\right)^{-1}, \tag{9}$$

where $\ell_p = \kappa/(k_B T)$ is the persistence length, with k_B being the Boltzmann constant. Here $\mu_{\mathrm{ph}} = 100 \kappa \ell_p / \ell_c^3$ is the effective stretch rigidity in the presence of thermal fluctuations. Interestingly, the limit $L \to \infty$ corresponds to a high molecular-weight analog of a phantom network, including node fluctuations. This slightly differs ($\sim 10\%$) from the limit of affinely deforming nodes with only transverse bending fluctuations [5, 12, 63]. For finite L we predict a strong L-dependence of the network elasticity that has not been identified by previous studies. Moreover, the non-affinity leads to a crucial correction to the non-linear stiffening effect [11, 12], as will be detailed in future work [65].

Above we have focused on 3D networks, but our theory is general to other dimensionalities. There is, however, an essential difference between 3D and 2D networks, due to the Maxwell isostatic condition for rigidity percolation for coordination number $z = Z_c = 2d$ in d dimensions [66]. For networks formed by long polymers the connectivity approaches 4 from below. The local, near isostatic connectivity in 2D leads to long-range floppy modes [49, 50] that are absent in 3D, for which there is always a local floppy mode (see Fig. 4(a)). In 2D networks, independent displacements of crosslinks are prohibited without stretching. In the limit of large μ, when one crosslink in a 2D network is displaced, all other crosslinks on its connected polymer must deform in a particular way to avoid stretching deformation (see Fig. 4(b)), leading to displacements of L/ℓ_c crosslinks. This *floppy-mode* deformation requires taking into account the coupled deformation of multiple crosslinks when calculating both the medium rigidity (Eq. (6)) and the coefficient tensor (Eq. (7)). We find that $K_\perp \sim L$ for a 2D lattice. For Mikado networks, $K_\perp$ is further enhanced by the broad distribution of crosslink separations ℓ_c along the backbone [49], resulting in $K_\perp \sim L^3$. As shown in Sec. IV
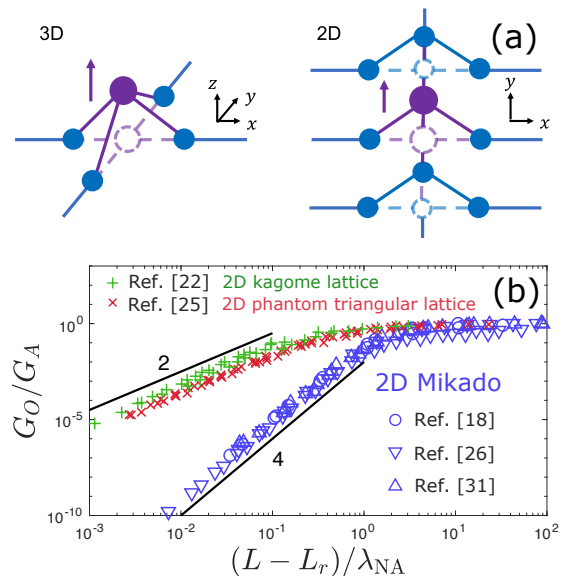

Figure 4. (a). Difference between 3D and 2D networks. In 3D networks, a crosslink can deform in the direction perpendicular to its two connected polymers, without deforming other crosslinks. In 2D networks, an entire polymer has to move together with the crosslink, leading to deformation of L/ℓ_c crosslinks. (b). Scaling dependence in 2D Mikado and 2D lattice-based networks. $\lambda_{\mathrm{NA}} = \kappa^{-1/4} \mu^{1/4} \ell_c^{3/2}$ for Mikado and $\lambda_{\mathrm{NA}} = \kappa^{-1/2} \mu^{1/2} \ell_c^2$ for lattice-based. $L_r = 5.9 \ell_c$ (Mikado), $2.94 \ell_c$ (phantom triangular) and $2.53 \ell_c$ (Kagome) are the minimum lengths for rigidity percolation. Simulation data reproduced from Ref. [19, 28, 35] (Mikado), Ref. [24] (Kagome lattice) and Ref. [27] (phantom triangular lattice). The slight difference between Ref. [24] and Ref. [27] is due to their different lattice structures.

of [63], we predict the following scaling dependences in the non-affine regime:

$$G_O \sim \begin{cases} L^2 & (\text{3D, any structure}) \\ L^2 & (\text{2D, lattice}) \\ L^4 & (\text{2D, Mikado}) \end{cases} \tag{10}$$

Equation (10) agrees with previous numerical studies for 3D lattices [22], 2D lattices [24, 27], and 2D Mikado networks [18, 19, 25, 28, 35], as shown in Fig. 4(b). While various molecular weight scalings of 2D Mikado networks have been reported, the previous numerical studies are consistent with a common $(L - L_r)^4$ (see Sec. IV of [63]). Interestingly, although the local network structure strongly affects the scaling dependence of 2D networks with different distributions of ℓ_c, our model predicts a L^2 scaling that is robust for any structure, including potentially broad, randomly distributed ℓ_c in experimentally relevant 3D networks. Previous experimental studies on hydrogels and numerical studies on 3D Mikado-like networks are consistent with an L^2 dependence in 3D [26, 39, 51].

In conclusion, the model presented above constitutes a

basis for understanding the linear elasticity of both thermal semiflexible polymer and athermal fiber networks in 2D and 3D, including non-affine effects. Such non-affine effects are known to be more important for such systems than for flexible polymer gels, although most prior work addressing non-affinity in such systems has been limited to simulation, particularly for 3D. As we have shown, the Maxwell isostatic condition results in an important difference between 2D and 3D networks, reinforcing the demand for a 3D theory. Our EMT approach predictions are in very good agreement with prior numerical simulations for athermal networks. In addition, we predict the elasticity of thermal networks and find an unexpectedly strong molecular weight dependence for which thermal simulations have been lacking. Our thermal results may aid ongoing experimental efforts to quantify non-affine effects, which have proven inconclusive to date in biopolymer networks.

An important feature of our theory is that the EMT is allowed to deform non-affinely, allowing us to capture accurately non-affine deformations of real networks. This also allows predictions of non-affine fluctuations including thermal fluctuations, in contrast to prior effective medium approaches. Our model can be extended to predict nonlinear elastic effects such as stress-stiffening [11, 12]. This is possible even with our assumptions above of small displacements, in a way similar to prior theories of nonlinear semiflexible chain stretching [5, 12, 67]. Our model can also be extended to address strain-controlled criticality that has previously been identified computationally [65]. However, an important limitation of our approach is that it is a mean-field theory, and cannot be expected to predict anomalous critical exponents. Moreover, with the Hamiltonian of Eq. (2), the derivation of network dynamics is straightforward. Finally, our EMT approach is not limited to permanently-crosslinked networks, and can be applied also to transiently-crosslinked networks [68–70]. Interestingly, in Refs. [60, 61] an effective spring constant, which is conceptually similar to our effective medium rigidity, is estimated for a solution of entangled polymers. When combined with the present model, this suggests a possible model for entangled solutions.

[1] D. Fletcher and R. Mullins, Nature **463**, 485 (2010).
[2] J. L. Shivers, J. Feng, A. S. G. van Oosten, H. Levine, P. A. Janmey, and F. C. MacKintosh, Proc. Natl. Acad. Sci. U.S.A. **117**, 21037 (2020).
[3] A. S. van Oosten, X. Chen, L. Chin, K. Cruz, A. E. Patteson, K. Pogoda, V. B. Shenoy, and P. A. Janmey, Nature **573**, 96 (2019).
[4] A. W. Hudnut, L. Lash-Rosenberg, A. Xin, J. A. Leal Doblado, C. Zurita-Lopez, Q. Wang, and A. M. Armani, ACS Biomater. Sci. Eng. **4**, 1916 (2018).
[5] F. C. MacKintosh, J. Käs, and P. A. Janmey, Phys. Rev. Lett. **75**, 4425 (1995).
[6] H. Isambert and A. Maggs, Macromolecules **29**, 1036 (1996).
[7] K. Kroy and E. Frey, Phys. Rev. Lett. **77**, 306 (1996).
[8] F. Gittes and F. C. MacKintosh, Phys. Rev. E **58**, R1241 (1998).
[9] B. Hinner, M. Tempel, E. Sackmann, K. Kroy, and E. Frey, Phys. Rev. Lett. **81**, 2614 (1998).
[10] D. C. Morse, Macromolecules **31**, 7030 (1998).
[11] M. L. Gardel, J. H. Shin, F. C. MacKintosh, L. Mahadevan, P. Matsudaira, and D. A. Weitz, Science **304**, 1301 (2004).
[12] C. Storm, J. J. Pastore, F. C. MacKintosh, T. C. Lubensky, and P. A. Janmey, Nature **435**, 191 (2005).
[13] D. Mizuno, C. Tardin, C. F. Schmidt, and F. C. MacKintosh, Science **315**, 370 (2007).
[14] O. Chaudhuri, S. H. Parekh, and D. A. Fletcher, Nature **445**, 295 (2007).
[15] O. Stenull and T. Lubensky, arXiv preprint arXiv:1108.4328 (2011).
[16] C. P. Broedersz and F. C. MacKintosh, Rev. Mod. Phys. **86**, 995 (2014).
[17] R. H. Pritchard, Y. Y. S. Huang, and E. M. Terentjev, Soft matter **10**, 1864 (2014).
[18] D. A. Head, A. J. Levine, and F. C. MacKintosh, Phys. Rev. Lett. **91**, 108102 (2003).
[19] J. Wilhelm and E. Frey, Phys. Rev. Lett. **91**, 108103 (2003).
[20] P. R. Onck, T. Koeman, T. Van Dillen, and E. van der Giessen, Phys. Rev. Lett. **95**, 178102 (2005).
[21] M. Das, F. C. MacKintosh, and A. J. Levine, Phys. Rev. Lett. **99**, 038101 (2007).
[22] C. P. Broedersz, M. Sheinman, and F. C. MacKintosh, Phys. Rev. Lett. **108**, 078102 (2012).
[23] A. Shahsavari and R. C. Picu, Phys. Rev. E **86**, 011923 (2012).
[24] X. Mao, O. Stenull, and T. C. Lubensky, Phys. Rev. E **87**, 042602 (2013).
[25] A. S. Shahsavari and R. C. Picu, Int. J. Solids Struct. **50**, 3332 (2013).
[26] V. D. Nguyen, A. Pal, F. Snijkers, M. Colomb-Delsuc, G. Leonetti, S. Otto, and J. van der Gucht, Soft Matter **12**, 432 (2016).
[27] A. J. Licup, A. Sharma, and F. C. MacKintosh, Phys. Rev. E **93**, 012407 (2016).
[28] K. Baumgarten and B. P. Tighe, Soft Matter **17**, 10286 (2021).
[29] M. Rubinstein and R. H. Colby, *Polymer Physics*, 1st ed. (Oxford, New York, 2003).
[30] H. M. James, J. Chem. Phys. **15**, 651 (1947).
[31] H. M. James and E. J. Guth, J. Chem. Phys. **11**, 455 (1948).
[32] P. J. Flory, Br. Polym. J. **17**, 96 (1985).
[33] C. Miehe, S. Göktepe, and F. Lulei, J. Mech. Phys. Solids **52**, 2617 (2004).

[34] A. Raina and C. Linder, J. Mech. Phys. Solids **65**, 12 (2014).

[35] D. A. Head, A. J. Levine, and F. C. MacKintosh, Phys. Rev. E **68**, 061907 (2003).

[36] J. S. Palmer and M. C. Boyce, Acta Biomater. **4**, 597 (2008).

[37] E. M. Huisman, C. Storm, and G. T. Barkema, Phys. Rev. E **78**, 051801 (2008).

[38] A. R. Cioroianu, E. M. Spiesz, and C. Storm, J. Mech. Phys. Solids **89**, 110 (2016).

[39] M. Islam and R. Picu, Journal of Applied Mechanics **85** (2018).

[40] J. C. Phillips, J. Non-Cryst. Solids **34**, 153 (1979).

[41] M. F. Thorpe, J. Non-Cryst. Solids **57**, 355 (1983).

[42] S. Feng, M. F. Thorpe, and E. Garboczi, Phys. Rev. B **31**, 276 (1985).

[43] C. P. Broedersz, X. Mao, T. C. Lubensky, and F. C. MacKintosh, Nat. Phys. **7**, 983 (2011).

[44] M. Sheinman, C. P. Broedersz, and F. C. MacKintosh, Phys. Rev. E **85**, 021801 (2012).

[45] X. Mao, O. Stenull, and T. C. Lubensky, Phys. Rev. E **87**, 042601 (2013).

[46] X. Mao, A. Souslov, C. I. Mendoza, and T. Lubensky, Nature Communications **6**, 1 (2015).

[47] J. Huang, J. O. Cochran, S. M. Fielding, M. C. Marchetti, and D. Bi, Phys. Rev. Lett. **128**, 178001 (2022).

[48] O. K. Damavandi, M. L. Manning, and J. M. Schwarz, EPL **138**, 27001 (2022).

[49] C. Heussinger and E. Frey, Phys. Rev. Lett. **97**, 105501 (2006).

[50] D. Zhou, L. Zhang, and X. Mao, Phys. Rev. Lett. **120**, 068003 (2018).

[51] M. Jaspers, M. Dennison, M. F. Mabesoone, F. C. MacKintosh, A. E. Rowan, and P. H. Kouwer, Nat. Commun. **5**, 1 (2014).

[52] B. P. Tighe, Phys. Rev. Lett. **109**, 168303 (2012).

[53] M. Yucht, M. Sheinman, and C. Broedersz, Soft Matter **9**, 7000 (2013).

[54] R. Milkus and A. Zaccone, Phys. Rev. E **95**, 023001 (2017).

[55] J. L. Shivers, A. Sharma, and F. C. MacKintosh, arXiv preprint arXiv:2203.04891 (2022).

[56] A. Sharma, A. J. Licup, K. A. Jansen, R. Rens, M. Sheinman, G. H. Koenderink, and F. C. MacKintosh, Nat. Phys. **12**, 584 (2016).

[57] M. F. J. Vermeulen, A. Bose, C. Storm, and W. G. Ellenbroek, Phys. Rev. E **96**, 053003 (2017).

[58] M. Merkel, K. Baumgarten, B. P. Tighe, and M. L. Manning, Proc. Natl. Acad. Sci. U.S.A. **116**, 6560 (2019).

[59] S. Arzash, J. L. Shivers, and F. C. MacKintosh, Soft Matter **16**, 6784 (2020).

[60] D. C. Morse, Phys. Rev. E **63**, 031502 (2001).

[61] H. Hinsch, J. Wilhelm, and E. Frey, Eur. Phys. J. E **24**, 35 (2007).

[62] M. Rubinstein and S. Panyukov, Macromolecules **35**, 6670 (2002).

[63] See Supplemental Material [url] for detailed derivations, which includes Refs. [71, 72].

[64] In principle the assumptions of homogeneity and isotropy are not required for the model. Here they are adopted for simplicity.

[65] S. Chen, T. Markovich, and F. C. MacKintosh, unpublished.

[66] J. C. Maxwell, Lond. Edinb. Dublin philos. mag. **27**, 294 (1864).

[67] J. F. Marko and E. D. Siggia, Macromolecules **28**, 8759 (1995).

[68] O. Lieleg, M. M. A. E. Claessens, Y. Luan, and A. R. Bausch, Phys. Rev. Lett. **101**, 108101 (2008).

[69] C. P. Broedersz, M. Depken, N. Y. Yao, M. R. Pollak, D. A. Weitz, and F. C. MacKintosh, Phys. Rev. Lett. **105**, 238101 (2010).

[70] S. Chen, C. P. Broedersz, T. Markovich, and F. C. MacKintosh, Phys. Rev. E **104**, 034418 (2021).

[71] J. R. Klauder, Ann. Phys. **14**, 43 (1961).

[72] K. A. Jansen, A. J. Licup, A. Sharma, R. Rens, F. C. MacKintosh, and G. H. Koenderink, Biophys. J. **114**, 2665 (2018).